Using Dispersed Modes During Model Correlation

Eric C. Stewart*, Megan L. Hathcock†
NASA, Marshall Space Flight Center, AL, 35812

The model correlation process for the modal characteristics of a launch vehicle is well established. After a test, parameters within the nominal model are adjusted to reflect structural dynamics revealed during testing. However, a full model correlation process for a complex structure can take months of man-hours and many computational resources. If the analyst only has weeks, or even days, of time in which to correlate the nominal model to the experimental results, then the traditional correlation process is not suitable. This paper describes using model dispersions to assist the model correlation process and decrease the overall cost of the process. The process creates thousands of model dispersions from the nominal model prior to the test and then compares each of them to the test data. Using mode shape and frequency error metrics, one dispersion is selected as the best match to the test data. This dispersion is further improved by using a commercial model correlation software. In the three examples shown in this paper, this dispersion-based model correlation process performs well when compared to models correlated using traditional techniques and saves time in the post-test analysis.

I. Introduction

To ensure vehicle safety during a launch, the vehicle controller is designed to maintain stability while accounting for uncertainty in many input parameters, among them the vehicle mode shapes and frequencies. NASA ensures that the vehicle maintains stability for a 10% frequency uncertainty in the first bending mode and 20% frequency uncertainty in all higher-order modes.[1] Similar to the flight controller the vehicle loads are dependent on the structural dynamics of the vehicle. While the design loads allow for analytical model uncertainties the vehicle modes must be well understood prior to flight.[2]

The vehicle modes are better understood through the vehicle component static and modal tests and the integrated vehicle modal tests. These modal test results are used to tune and correlate the vehicle structural models that feed the loads calculations and controller design. This correlation reduces the uncertainty in the integrated model and provides added confidence that the loads and the controller are using the best structural model.

In previous launch vehicle programs modal testing of a launch vehicle occurred early in the program to allow for the vehicle to be tested in a variety of configurations. The vehicle structural models were correlated to the data and the overall uncertainty in the structural model is reduced.

However, the NASA Space Launch System will forgo the traditional modal testing approach in favor of a modal testing program that emphasizes testing of vehicle components. The fully integrated vehicle will not have modal test data until it is stacked inside the vehicle assembly building (VAB) at Kennedy Space Center (KSC) and the vehicle and mobile launcher are modally tested as an integrated system. But the modal tests are close in time to the Flight Readiness Review (FRR), so a fully correlated vehicle flight model will not inform the loads or controls analysis before flight.

The current focus of this work is to devise a methodology to incorporate modal test data into vehicle models within weeks of testing. The method presented in this paper begins by creating many dispersions of the nominal test model. The model dispersion that best matches the test data is refined by tuning it manually or with commercial software. The refined dispersion is known as the Best Model Estimate (BME)

*AST, Structural Dynamics, NASA MSFC; eric.c.stewart-1@nasa.gov, AIAA Member
†NASA Pathways Intern, NASA MSFC; megan.l.hathcock@nasa.gov

of the test data. The advantage of the dispersed modes correlation methodology is that it saves time during the post-test correlation while still producing a correlated model. This occurs by creating the dispersed models before the test and then seeding the model fine-tuning with a dispersed model that best matches the structural dynamics seen during testing. What follows in this paper is a description of the model dispersion process, the selection of the BME, and the use of the model tuning software. Three structures are used to prove out the dispersed modes process: a small utility cart, the Test Article Unit for Rectified Systems Testing (TAURUS-T, hereafter referred to as TAURUS) , and the Ares I-X launch vehicle.[3]

II. Models

A. Cart

The steel cart used as the first test case is shown in Fig. 1. The cart is about 4 ft long, 2.5 ft wide, and 3 ft tall and weighs around 156 lbs. It has four wheel assemblies bolted to two supporting beams that run the width of the cart. The supporting beams are connected to the bottom shelf with three evenly-spaced, one-inch welds on either side of each beam, shown in red in Fig. 2a. The cart shelves are made of 0.12 inch thick steel sheets with of a space of 20 inches between the top and bottom shelf. A supporting beam runs along the length of the top shelf and connects to the shelf with four evenly-spaced, one-inch welds on either side. The welds are illustrated in red on the top shelf of Fig. 2a. The corners of the cart, highlighted in Fig. 1 welded only around the outside perimeters where the shelves meet the angle iron legs as shown in blue in Fig. 2a. The handle is a hollow circular tube that is welded to the back two legs. To decease high frequency rattle, room temperature vulcanization silicone, (RTV), was placed along the edge of each supporting beam, which is illustrated by the yellow dotted lines in Fig. 2a.

Figure 1: Cart and corner connection

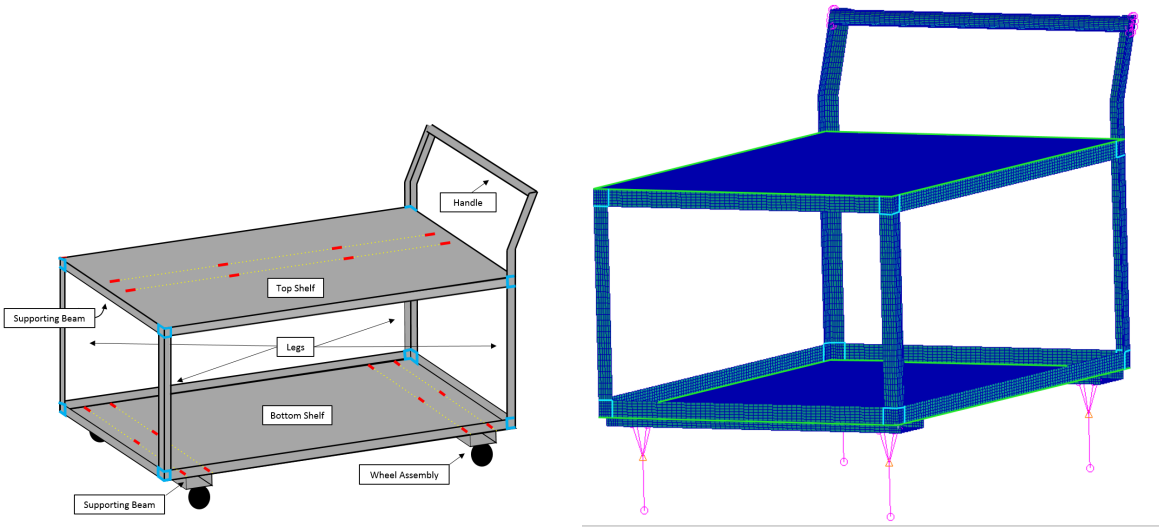

(a) Illustrated cart with labels, welds, and RTV

(b) Cart finite element model

Figure 2: Description of the cart and finite element model

The cart is modeled with finite elements using MSC PATRAN/NASTRAN as shown in Fig. 2b. The top shelf, bottom shelf, three support beams, and legs are modeled using shell elements. A fine mesh is used around the corners and edges of the cart so that small strips of elements can be grouped together and used to tune the model. The top and bottom shelve elements are equivalenced along the green lines to represent the solid connections of the cart shelf edges. The corner elements are not equivalenced to match actual cart configuration. The welds connecting the shelves with their respective support beams are modeled by equivalencing the nodes between the shelves and the beams where the welds would go. All nodes between the shelves and beams that are not equivalenced are connected with six degree of freedom springs to represent the RTV. Since the spring stiffness of the RTV in these joints is unknown, stiff placeholder values are used. The leg elements are equivalenced to the shell elements along the light blue lines shown in Fig. 2b. The handle is modeled using bar elements with a circular cross-section and is connected to the leg elements using two multipoint constraints as shown in pink in Fig. 2b.

The wheels are modeled as rigid elements that connect the cart to a six degree of freedom spring that is connected to ground. As shown in Fig. 3, Nodes 1 through 4 are placed in the model where the wheel assembly bolts to the actual cart. A point mass equal to the weight of the assembly is placed at Node 7, the approximate center of gravity of the wheel assembly. The spring stiffness of the wheel assemblies is unknown, therefore stiff placeholder values are used for the translational and rotational degrees of freedom and are then tuned during model correlation.

Using the NASTRAN design optimization Solution 200 , the sensitivity of the design variables on each mode frequency is determined. Since the element thicknesses and material properties are well known, the unknown spring stiffness placeholders are tuned first in accordance with their reported sensitivities. Through an iterative process the placeholder values and some material and physical properties are tuned to make the model frequencies more closely match the test mode frequencies to create a "hand-tuned" model. The first 10 frequencies of the nominal and hand-tuned models as well as the first 8 frequencies of the test modes are shown in Table 1. The first two model modes are observed during the test but are not reported here due to questionable data quality.

The modal assurance criteria (MAC)[4] between the nominal model and test modes is shown in Table 2. The MAC between the hand-tuned model and test modes are shown in Table 3. Each test mode in the left column is compared with the finite element model (FEM) modes in the top row. The pair that produces the highest MAC value is used to calculate frequency error. For example, in Table 2 test mode 3 has the highest MAC value when compared with fem mode 7. The frequency error between test mode 3 and FEM mode 7 is calculated and placed in the right most column. The MAC values in the tables below are colored

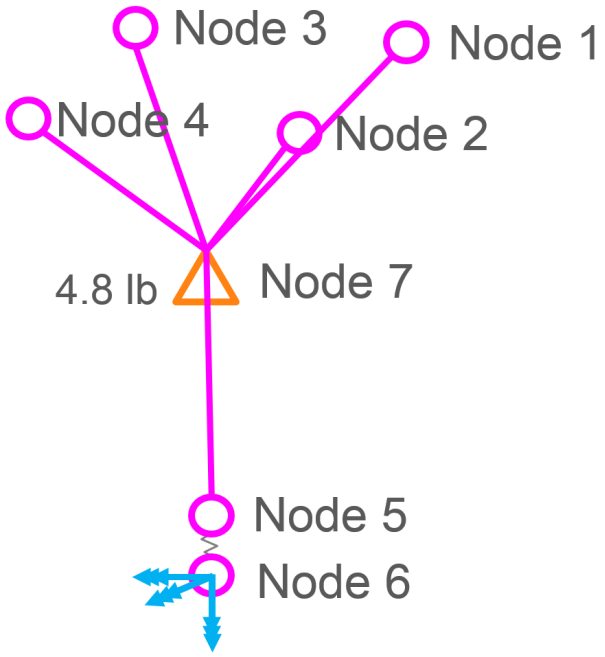

Figure 3: Wheel assembly model

Table 1: Table of Cart nominal modal, tuned model, and test modes

Nominal Model Modes (Hz)	Hand-Tuned Model Modes (Hz)	Test Modes (Hz)
7.50	1.56	—
9.10	15.05	—
14.59	22.07	23.8
16.07	25.43	24.3
22.56	31.39	29.1
25.48	43.13	40.7
26.49	47.27	45.3
42.04	47.41	47.4
46.65	50.18	51.0
53.26	56.74	53.8

from dark to light with dark green being the highest values and white being the lowest values. Similarly, the frequency errors are colored from red to green with red being the highest value and green being the lowest value. As expected, the nominal model with all of the untuned place holder values poorly matches the test modes. However, the MAC between the hand-tuned modes and test modes shows a significant improvement with the frequency error decreased to 4.66% and MAC diagonal values all above 0.9.

Table 2: MAC: Nominal cart modes vs test modes

	Nominal Model Modes									
Test Modes	Freq(Hz)		26.5	16.1	42.0	14.6	22.6	25.5	53.3	46.7	
		Mode	7	4	6	3	5	8	10	9	Freq % Diff
	23.8	3	0.69	0.00	0.00	0.24	0.00	0.00	0.00	0.00	11.5
	24.3	4	0.01	0.62	0.01	0.00	0.00	0.00	0.03	0.03	33.8
	29.1	5	0.00	0.00	0.62	0.00	0.17	0.00	0.00	0.00	44.3
	40.7	6	0.18	0.00	0.03	0.42	0.00	0.00	0.00	0.00	64.1
	45.3	7	0.00	0.00	0.09	0.00	0.10	0.00	0.00	0.01	50.2
	47.4	8	0.00	0.03	0.00	0.00	0.00	0.62	0.10	0.05	46.2
	51.0	9	0.00	0.00	0.00	0.01	0.00	0.03	0.48	0.00	4.4
	53.8	10	0.00	0.00	0.00	0.00	0.00	0.04	0.27	0.01	13.3
									Freq % Diff Avg		33.48

Table 3: MAC: Hand-tuned cart modes vs test modes

	Hand-Tuned Model Modes									
Test Modes		Freq(Hz)	22.1	25.4	31.4	43.1	47.3	47.4	50.2	56.7	
	Freq(Hz)	Mode	3	4	5	6	7	8	9	10	Freq % Diff
	23.8	3	0.98	0.00	0.00	0.00	0.00	0.00	0.00	0.00	7.1
	24.3	4	0.01	0.93	0.00	0.00	0.00	0.00	0.00	0.00	4.7
	29.1	5	0.00	0.00	0.93	0.02	0.01	0.00	0.00	0.00	7.8
	40.7	6	0.00	0.00	0.03	0.92	0.01	0.00	0.00	0.00	6.1
	45.3	7	0.00	0.00	0.00	0.01	0.90	0.00	0.00	0.00	4.4
	47.4	8	0.00	0.00	0.00	0.00	0.00	0.91	0.00	0.05	0.1
	51.0	9	0.01	0.00	0.00	0.00	0.00	0.00	0.96	0.01	1.7
	53.8	10	0.00	0.00	0.00	0.00	0.00	0.02	0.00	0.94	5.4
									Freq % Diff Avg		4.66

B. TAURUS-T

The TAURUS, shown in Fig. 4, is an apparatus primarily used as an educational and training tool at Johnson Space Center. The TAURUS is seven feet tall and six feet wide, made of Unistrut bars connected by brackets, and bolted to an isolated mass to approximate cantilevered boundary conditions.

Figure 4: Picture of the TAURUS setup

The TAURUS is modeled in NASTRAN using bar elements with a u-shaped channel cross section. The bar elements are connected together using spring elements with a finite length to prevent coincident nodes and correct for the fact that the Unistrut bars are not connected at their shear centers. The hand-tuned spring stiffnesses are determined by modeling the brackets and determining their deflections for different load cases. The tuned spring stiffnesses greatly improve the accuracy of the TAURUS over the nominal model as seen by comparing the first 15 mode frequencies in Table 4. Test frequencies 1-6 are higher than either of the models, indicating that the model is soft, despite the tuned springs, however, test mode frequencies 7-10 are smaller than the model modes and the associate mode shape MAC values are generally small. So the finite element model likely has deficiencies and needs improvement.

Table 4: Table of TAURUS modes, both analytical and test

Mode	Test (Hz)	Tuned Model (Hz)	Nominal Model (Hz)
1	4.92	3.36	2.87
2	6.60	5.02	4.40
3	7.58	5.65	4.83
4	28.99	27.06	24.11
5	29.37	27.85	26.74
6	31.40	30.88	28.63
7	34.76	38.46	33.14
8	41.10	43.82	44.81
9	43.81	47.14	44.85
10	49.60	49.92	48.74
11	52.38	53.46	52.48
12	55.16	61.66	54.04
13	71.81	67.54	65.79
14	74.76	72.68	67.97
15	79.69	75.68	69.41

Table 5 shows the MAC and frequency error between the nominal model and the test modes while Table 6 shows the MAC and frequency error between the test modes and the hand-tuned model. The hand-tuned model with adjusted spring stiffnesses provides a significant improvement over the nominal model in both frequency and mode shape errors.

Table 5: Modal assurance criteria (MAC) between TAURUS test data and nominal model

Mac: Test vs Uncorrelated Model (Disp 1)												
Test Modes	Model Modes											
		Freq(Hz)	2.87	4.40	4.83	24.11	28.63	26.74	33.14	44.85	44.81	52.48	
	Freq(Hz)	Mode	1	2	3	4	6	5	7	9	8	11	Freq % Diff
	4.92	1	0.99	0.00	0.00	0.00	0.00	0.00	0.00	0.00	0.00	0.00	41.8
	6.60	2	0.00	0.99	0.00	0.00	0.00	0.02	0.00	0.02	0.00	0.01	33.4
	7.58	3	0.00	0.00	0.99	0.01	0.00	0.00	0.00	0.00	0.00	0.00	36.4
	28.99	4	0.00	0.00	0.00	0.47	0.27	0.16	0.02	0.00	0.03	0.01	16.8
	29.37	5	0.00	0.00	0.00	0.20	0.64	0.00	0.00	0.00	0.07	0.00	2.5
	31.40	6	0.00	0.00	0.00	0.11	0.05	0.75	0.03	0.00	0.00	0.04	14.8
	34.76	7	0.00	0.00	0.00	0.00	0.00	0.03	0.94	0.01	0.00	0.00	4.6
	41.10	8	0.00	0.01	0.00	0.00	0.00	0.15	0.01	0.65	0.00	0.08	9.1
	43.81	9	0.00	0.00	0.00	0.00	0.25	0.00	0.00	0.00	0.52	0.00	2.3
	49.60	10	0.00	0.00	0.00	0.00	0.01	0.02	0.00	0.19	0.01	0.59	5.8

Table 6: Modal assurance criteria (MAC) between TAURUS test data and hand-tuned model

Mac: Test vs Hand Tuned Model												
	Model Modes											
		Freq(Hz)	3.36	5.02	5.65	27.85	27.06	30.88	38.46	43.82	47.14	49.92	
Test Modes	Freq(Hz)	Mode	1	2	3	5	4	6	7	8	9	10	Freq % Diff
	4.92	1	0.99	0.00	0.00	0.00	0.00	0.00	0.00	0.00	0.00	0.00	31.74
	6.60	2	0.00	0.99	0.00	0.00	0.00	0.01	0.00	0.02	0.00	0.00	24.00
	7.58	3	0.00	0.00	0.99	0.01	0.00	0.00	0.00	0.00	0.00	0.00	25.50
	28.99	4	0.00	0.00	0.00	0.47	0.32	0.16	0.02	0.00	0.00	0.00	3.91
	29.37	5	0.00	0.00	0.00	0.20	0.75	0.00	0.00	0.00	0.00	0.00	7.89
	31.40	6	0.00	0.01	0.00	0.11	0.06	0.76	0.03	0.00	0.00	0.01	1.66
	34.76	7	0.00	0.00	0.00	0.00	0.00	0.04	0.94	0.01	0.00	0.00	10.65
	41.10	8	0.00	0.01	0.00	0.00	0.00	0.09	0.01	0.90	0.00	0.02	6.60
	43.81	9	0.00	0.00	0.00	0.00	0.01	0.00	0.00	0.00	0.55	0.00	7.62
	49.60	10	0.00	0.00	0.00	0.00	0.00	0.01	0.00	0.00	0.06	0.61	0.64

C. Ares I-X

As described by Horta, et al.,[5] the Ares I-X flight vehicle model consists of three main parts, the First Stage (FS), the Upper Stage Simulator (USS), and mass simulators to represent the Crew Module (CM) and Launch Abort System (LAS). A MSC NASTRAN model is created by attaching the FS, USS, and CM/LAS models with rigid elements at each interface. The vehicle skin is modeled using shell elements while section flanges and braces are modeled using beam elements. Springs are used to model the interface between the joints on the upper stage and first stage segments as well as the ground and non-flight hardware interfaces. The finite element model of the Ares I-X is shown in Fig. 5.

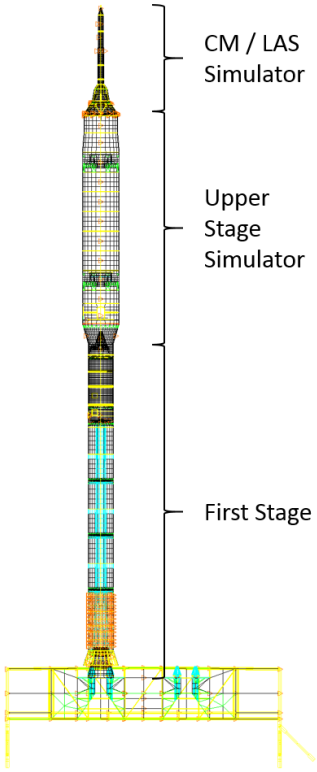

Figure 5: Ares I-X Finite Element Model

Using sensitivities, potential sources of uncertainty, and a mass verification exercise, Horta, et al. chose eight parameters for model correlation: the USS joint stiffness, Young Moduli for the USS, LAS, First Stage,

Aft Skirt (stiffeners and shell), Forward Skirt Extension, and Frustum. Modulus of elasticity is allowed to vary by ±10%, while USS joint stiffness is allowed to vary by ±50%. The first 14 frequencies of the nominal model, tuned model, and the test modes are shown in Table 7.

Table 7: Table of Ares I-X nominal modal, tuned model, and test modes

Nominal Model Modes (Hz)	Tuned Model Modes (Hz)	Test Modes (Hz)
0.18	0.18	0.18
0.22	0.22	0.22
1.02	1.05	1.06
1.17	1.21	1.19
1.87	1.87	1.84
2.66	2.67	2.06
3.25	3.38	3.45
3.49	3.52	3.64
3.50	3.64	3.67
3.58	3.69	4.61
4.22	4.23	4.78
4.66	4.67	6.18
4.78	4.82	6.41
4.84	4.87	6.66

The MACs between the nominal model and test modes is shown in Table 8. The MAC between the tuned model and test modes is shown in Table 9. Test modes in the left column are compared with nominal model modes in the top row. Pairs with high MAC values are considered matches to use for calculating frequency error. For example, test mode 13 and fem mode 16 are considered a match due to their high MAC value, as shown in Fig. 8. The MAC values between the nominal model modes and test modes are high, but the tuned model decreases the frequency error.

Table 8: MAC: Nominal Ares I-X modes vs test modes

Test Modes	Nominal Model Modes																						
	Freq (Hz)		0.18	0.22	1.02	1.17	1.87	2.66	3.25	3.49	3.50	3.58	4.22	4.66	4.78	4.84	4.92	6.01	6.24	6.44	6.69	8.98	
		Mode	1	2	3	4	5	6	7	8	9	10	11	12	13	14	15	16	17	18	19	20	Freq % Diff
	0.18	1	0.90	0.01	0.39	0.02	0.20	0.02	0.28	0.01	0.05	0.63	0.11	0.28	0.22	0.08	0.26	0.08	0.09	0.02	0.01	0.01	4.7
	0.22	2	0.00	0.99	0.00	0.45	0.01	0.31	0.00	0.11	0.39	0.01	0.08	0.14	0.00	0.31	0.17	0.00	0.10	0.07	0.02	0.00	1.0
	1.06	3	0.47	0.00	1.00	0.00	0.42	0.00	0.68	0.01	0.00	0.05	0.22	0.24	0.42	0.00	0.15	0.16	0.00	0.01	0.01	0.00	3.8
	1.19	4	0.00	0.45	0.00	1.00	0.01	0.57	0.00	0.16	0.67	0.00	0.12	0.21	0.00	0.42	0.24	0.00	0.12	0.09	0.04	0.00	1.2
	1.84	5	0.00	0.26	0.00	0.59	0.02	0.90	0.00	0.14	0.54	0.00	0.04	0.16	0.00	0.33	0.23	0.00	0.14	0.09	0.03	0.00	44.9
	2.06	6	0.15	0.00	0.35	0.00	0.77	0.00	0.45	0.04	0.00	0.01	0.05	0.12	0.26	0.00	0.12	0.14	0.00	0.01	0.00	0.00	9.2
	3.45	7	0.32	0.00	0.66	0.01	0.42	0.00	0.99	0.07	0.00	0.01	0.46	0.51	0.80	0.01	0.36	0.48	0.03	0.02	0.03	0.01	6.0
	3.64	8	0.11	0.26	0.00	0.48	0.01	0.52	0.00	0.03	0.74	0.21	0.06	0.25	0.00	0.61	0.36	0.00	0.33	0.23	0.10	0.02	35.0
	3.67	9	0.03	0.34	0.00	0.62	0.01	0.68	0.00	0.27	0.92	0.09	0.22	0.39	0.00	0.80	0.47	0.00	0.44	0.32	0.12	0.04	4.9
	4.61	10	0.18	0.09	0.28	0.13	0.14	0.14	0.53	0.13	0.23	0.01	0.60	0.96	0.65	0.33	0.89	0.51	0.35	0.03	0.00	0.06	1.2
	4.78	11	0.10	0.18	0.15	0.27	0.13	0.32	0.25	0.05	0.55	0.01	0.00	0.01	0.38	0.64	0.07	0.33	0.37	0.56	0.29	0.03	1.3
	6.18	12	0.15	0.03	0.24	0.03	0.18	0.04	0.34	0.07	0.10	0.04	0.14	0.06	0.55	0.14	0.02	0.62	0.12	0.18	0.02	0.00	22.5
	6.41	13	0.06	0.00	0.07	0.00	0.07	0.00	0.26	0.00	0.00	0.02	0.18	0.33	0.63	0.00	0.28	0.94	0.05	0.09	0.13	0.03	6.2
	6.66	14	0.01	0.06	0.01	0.08	0.01	0.16	0.01	0.06	0.30	0.01	0.05	0.18	0.02	0.61	0.30	0.02	0.89	0.80	0.36	0.19	6.3
																						Freq % Diff Avg	10.59

Table 9: MAC: Tuned Ares I-X modes vs test modes

Test Modes	Tuned Model Modes																					
	Freq (Hz)		0.18	0.22	1.05	1.21	1.87	2.67	3.38	3.52	3.64	3.69	4.23	4.67	4.82	4.87	4.92	6.27	6.46	6.63	7.02	9.01	
		Mode	1	2	3	4	5	6	7	8	9	10	11	12	13	14	15	16	17	18	19	20	Freq % Diff
	0.18	1	0.90	0.01	0.39	0.02	0.20	0.02	0.28	0.01	0.05	0.63	0.10	0.25	0.22	0.08	0.24	0.05	0.11	0.04	0.01	0.01	2.0
	0.22	2	0.00	0.99	0.00	0.45	0.01	0.29	0.00	0.01	0.38	0.01	0.09	0.18	0.00	0.31	0.20	0.00	0.05	0.06	0.01	0.00	2.4
	1.06	3	0.47	0.00	1.00	0.00	0.42	0.00	0.67	0.11	0.00	0.06	0.21	0.19	0.42	0.00	0.12	0.11	0.02	0.00	0.01	0.00	1.0
	1.19	4	0.00	0.45	0.00	1.00	0.01	0.54	0.00	0.02	0.66	0.00	0.14	0.26	0.00	0.41	0.28	0.00	0.06	0.07	0.02	0.00	1.9
	1.84	5	0.00	0.26	0.00	0.59	0.02	0.91	0.00	0.02	0.54	0.00	0.05	0.20	0.00	0.32	0.25	0.00	0.09	0.09	0.02	0.01	45.2
	2.06	6	0.15	0.00	0.34	0.00	0.77	0.00	0.45	0.14	0.00	0.01	0.06	0.09	0.25	0.00	0.09	0.11	0.02	0.00	0.00	0.00	9.1
	3.45	7	0.32	0.00	0.66	0.01	0.42	0.00	0.99	0.23	0.00	0.01	0.46	0.43	0.80	0.01	0.30	0.39	0.11	0.00	0.03	0.00	2.2
	3.64	8	0.11	0.26	0.00	0.48	0.01	0.50	0.00	0.00	0.74	0.20	0.06	0.32	0.00	0.60	0.41	0.00	0.21	0.24	0.07	0.01	35.0
	3.67	9	0.03	0.34	0.00	0.62	0.01	0.64	0.00	0.03	0.93	0.10	0.26	0.48	0.00	0.80	0.54	0.01	0.27	0.33	0.07	0.03	1.0
	4.61	10	0.18	0.09	0.28	0.13	0.14	0.13	0.54	0.14	0.23	0.01	0.61	0.91	0.66	0.33	0.84	0.42	0.52	0.09	0.00	0.04	1.3
	4.78	11	0.10	0.18	0.15	0.27	0.13	0.30	0.25	0.02	0.56	0.02	0.00	0.05	0.37	0.64	0.13	0.33	0.11	0.52	0.24	0.03	1.9
	6.18	12	0.15	0.03	0.24	0.03	0.18	0.04	0.35	0.31	0.10	0.04	0.12	0.02	0.55	0.14	0.00	0.66	0.01	0.22	0.01	0.00	22.0
	6.41	13	0.06	0.00	0.07	0.00	0.07	0.00	0.27	0.03	0.00	0.02	0.18	0.27	0.64	0.00	0.22	0.94	0.30	0.02	0.17	0.02	2.1
	6.66	14	0.01	0.06	0.01	0.08	0.01	0.15	0.01	0.00	0.32	0.01	0.06	0.23	0.02	0.62	0.36	0.04	0.61	0.96	0.28	0.18	2.9
																				Freq % Diff Avg			9.28

III. Model Tuning Methodology

A. Model dispersions

Model dispersions are created by taking the nominal test model and applying uncertainty factors to the stiffness parameters in the model. The stiffness parameters for a given model consist of material stiffness and spring rates. Each of the selected stiffness properties are independently and randomly varied to produce the dispersions. The variations in the stiffness parameters are customized for each model with the goal to account for model deficiencies through the dispersions.

The model dispersions are compared to the test mode frequencies and mode shapes. The model dispersion to test data comparison requires modal frequency and mode shape comparisons. The metric to determine the overall frequency error between the k^{th} dispersion and test frequencies is

$$g_1^k = \frac{1}{N}\sum_{i=1}^{N} W_i \left| \frac{f_i^{test} - f_i^{dispersion}}{f_i^{test}} \right| \times 100 \tag{1}$$

which is the average absolute relative error between the k^{th} dispersion and the test data. The value f_i^{test} is the i^{th} test frequency being used for comparison, $f_i^{dispersion}$ is the corresponding model dispersion frequency, N is the number of frequencies used in the comparison. The compared test and model mode frequencies are selected based on the of the mode shapes, as discussed below. The term W_i is a weighting factor that indicates the relative importance of test modes to the structural dynamics of interest during the model correlation procedure. Some test modes do not affect the load-bearing portions of the structure while others have high frequencies and are generally considered less trustworthy due to lower levels of excitation during the test. For instance, modes with a frequency of greater than 100Hz would be given a small weighting factor if the frequency range of interest is below 100Hz. Similarly, localized shell modes would be deweighted.

The mode shape comparison may use either the modal assurance criteria or cross orthogonality (XOR)[6]between the model dispersion and the test data as

$$g_2^k = \begin{cases} \left[[I] - [W]\,\Phi_{test}^T M_{aa}^k \Phi_{model}^k\right]_e & Cross\,Orthogonality \\ \left[[I] - [W]\,\dfrac{\left(\Phi_{test}^T \Phi_{model}^k\right)^2}{\left(\Phi_{test}^T \Phi_{test}\right)\left(\left(\Phi_{model}^k\right)^T \Phi_{model}^k\right)}\right]_e & MAC \end{cases} \tag{2}$$

where Φ_{test} are the test modes at the sensor locations, Φ_{model}^k are the modes of the k^{th} dispersion before matrix reductions, and M_{aa} is the Guyan reduction[7] of the dispersed model mass matrix that retains only the sensor location degrees of freedom as physical nodes. The mode weights are represented as a diagonal

matrix $[W]$. The mode shape comparisons are reduced to a single number using the Euclidean norm of the matrix, denoted as $[]_e$. The Euclidean norm accounts for both the on-diagonal and off-diagonal errors.

When comparing the model dispersion to the test data, MAC/XOR matrices are sorted to keep the highest values along the diagonal of the matrix. If there are more model modes than test modes, the process picks the best matching model modes to create a square MAC or XOR matrix. To start the maximum MAC/XOR values for each test mode are identified, and their associated analysis modes are reported. If there is a repeat in the associated analysis modes, meaning more than one test mode is matching with a single analysis mode, the analysis mode and test mode with the higher MAC/XOR is kept. The other test mode is then paired with the analysis mode that gives the next highest MAC value. The associated analysis modes are checked again, and the process is repeated until each test mode is matched with a single analysis mode. Once there are an equal number of test and analysis modes, the analysis modes are sorted to correspond with their matching test modes. This process ensures that modes can be tracked though the dispersion process and "mode swapping" does not cause errors .

When comparing the dispersed models to the test modal data with two metrics, a set of dispersions become the models that "best" match the data. This is due to the multi-objective approach where two objective functions are minimized. This set of non-dominated optimal models is known as a Pareto front.[8] After defining the Pareto front, one point needs to be selected as the starting point for further model tuning using the commercial software Attune from ATA Engineering . Thus a set of criteria is defined by the analysts to pick a dispersed model as the "best". The tie-break criteria includes, but it not limited to:

- Closeness to the original model
- Using the partial stack modal test data
- Using a transient response analysis of the test to match closeness
- Changing the weighting factors

Once the dispersion has undergone further model tuning, it is known as the Best Model Estimate (BME) of the test data.

B. Attune Correlation Software

Attune from ATA Engineering[9] is a MATLAB-based tool to assess the correlation of a model to test data and for updating the model to improve correlation. It uses structural dynamic modification[10] to update the model using a genetic algorithm. Attune improves the model frequencies and mode shapes with minimum changes in the design variables. For the purposes of this paper, the design variables are the parameters in a given model that are perturbed to create the dispersions. The genetic algorithm objective function is a combination of the RSS of the frequency errors and the RSS of the MAC (or XOR) on-diagonal error.

The root sum square (RSS) of the matrix diagonal accounts for the on-diagonal errors and neglects the off-diagonal errors. The RSS matrix norm of the modal assurance criteria matrix is

$$g_2 = [[I] - [W][MAC]]_{rss} = \sqrt{\sum_{i=1}^{N} [1 - MAC(i,i)]^2} \tag{3}$$

The RSS error metric can also use cross orthogonality by simply replacing the MAC terms in Eq. 3 with XOR terms.

IV. Method Comparison

A. Cart

For the cart model dispersions, all Young's moduli and densities are randomly varied with a uniform distribution between ±20%, while element thicknesses vary between ±30%. The material property values and regions of this application for the cart are shown in Fig. 6. The entire cart is made out of cold rolled steel, however, the material properties of the cart have been broken down into three regions: edges, corners, and

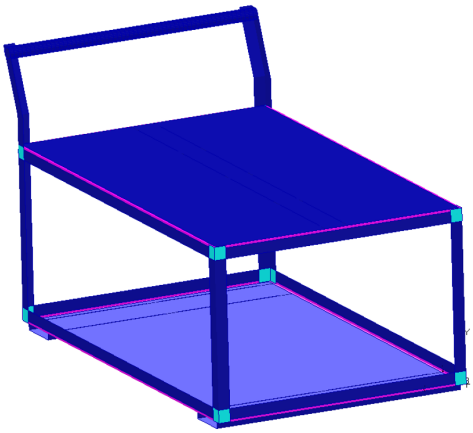

Cart Material Properties				
Color	Group	Property	Int. Value	Units
	Mat 1	E	2.90E+07	psi
		Rho	0.283	lb/in.³
	Mat 2	E	2.90E+07	psi
		Rho	0.20874	lb/in.³
	Mat 3	E	2.90E+07	psi
		Rho	0.283	lb/in.³
Dispersed ± 20%				

Figure 6: Nominal, untuned cart material properties

everything else. The edge and corner material property regions act as tuning knobs to adjust for unknown interface stiffnesses in the welded corner connections and bent edges. Only Young's modulus and density are allowed to change in these regions. The thicknesses on all parts of the cart are varied as well, property values and regions of this application are shown in Fig. 7. For the dispersions process, all springs in the model are

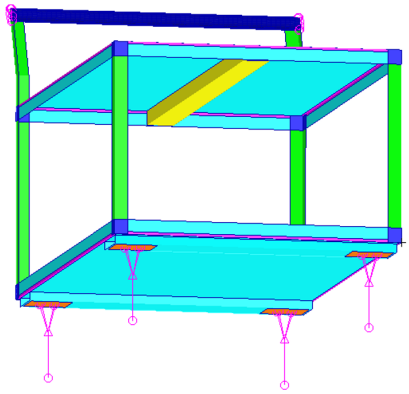

Cart Physical Properties			
Color	Property	Int. Value	Units
	Top Beam Thickness	0.103	in.
	Leg Thickness	0.2	in.
	Shelve Thickness	0.12	in.
	Handle Diameter	0.68	in.
	(OD/ID)	0.61	in.
	Wheel Plate Thickness	0.34	in.
	Edge Thickness	0.12	in.
	Corner Thickness	0.16	in.
Dispersed ± 30%			

Figure 7: Nominal, untuned cart physical properties

grouped into the three regions shown in Fig. 8. Each degree of freedom for these three springs groups is treated as an independent variable and randomly varied with a normal distribution between ±100%. Springs properties are distributed over a much larger design space than the material and physical properties because the spring constants are not well defined for the untuned model.

A roving accelerometer impact test was performed by MSFC on the cart in a grounded setup with the cart wheels were constrained to keep them from rolling or rotating in any direction. From the frequency response functions generated during the modal test, mode shapes and frequencies are calculated up to 80Hz using standard methods.

5000 dispersed cart models are created and their mode frequencies and shapes are calculated up to 60 Hz. For the dispersions plotted in Fig. 9, only analysis modes 3 through 10 are compared with the test data. Dispersions are plotted based on their frequency and mode shape error, the criteria of which is discussed above. The untuned model is shown in Fig. 9 as a black dot, while the hand-tuned model is shown as a yellow square. After plotting the dispersions using a Euclidean norm, the Pareto points, shown in green, can be determined by finding points that minimize frequency and mode shape error. The Pareto points alone show a significant improvement over the untuned model in both frequency and mode shape error.

The untuned model is used as a starting point for Attune optimization and put through three iterations,

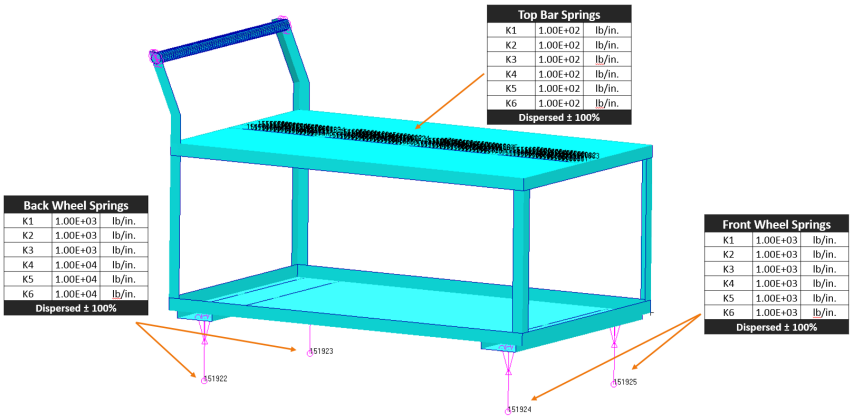

Figure 8: Untuned cart spring stiffnesses

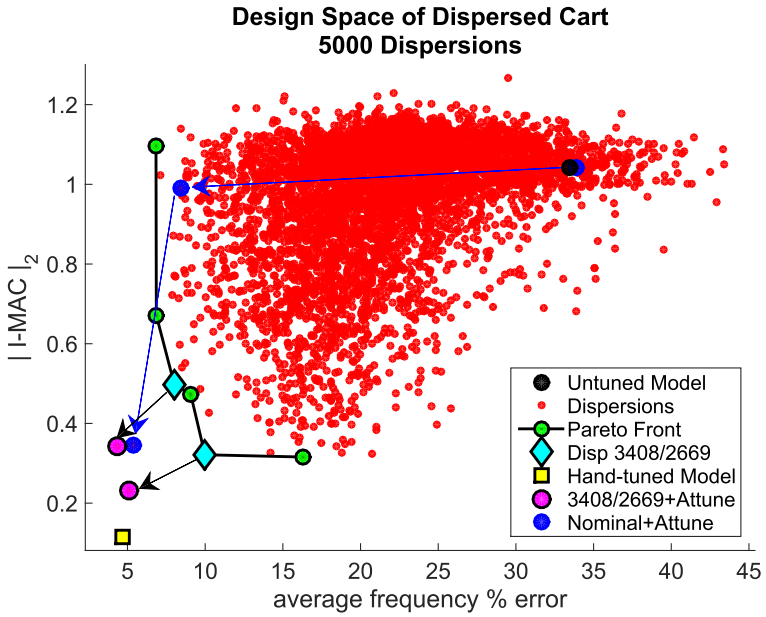

Figure 9: Cart dispersions plotted against the mode frequency and mode shape error metrics

which are shown by the blue dots in Fig. 9. The path between each iteration is traced with a blue arrow. Two Pareto points, dispersions 3408 and 2669, are chosen to go through one iteration of the Attune optimization process, the results of which are shown by the magenta dots. Black arrows connect the Pareto points and their Attune optimized counterparts. During the Attune optimization process for the untuned and chosen Pareto models, all Young's moduli, densities, thicknesses, and spring constants used to create the model dispersions are treated as design variables. Material and physical design variables are allowed to vary ±20% from the dispersion. Spring design variables are allowed to vary from 0% to 2000% of the dispersed value. The Attune optimized untuned model surpasses the all Pareto points with a lower RSS error. However, both Attune optimized Pareto models out perform the Attune optimized untuned model. All three Attune optimized models come very close to the hand-tuned model and show significant improvement in frequency and shape error over the untuned model.

It takes approximately 150 man-hours to create the hand-tuned correlated cart model. This involved performing the model sensitivity analysis for each model update and comparing the updated models to the test data. By comparison, the dispersion based model correlation process only takes a few days for this cart model and still creates a tuned model that accurately predicts the mode frequencies and shapes.

B. TAURUS

Dispersions of the TAURUS model start with the untuned model. In the dispersions the material Young's modulus and density are allowed to vary ±5% while each degree of freedom in the ten springs are treated as independent variables and are randomly varied with a uniform distribution between 10%-1000% of the nominal, untuned values. The large spring rate uncertainty values are set such that the hand-tuned model falls within the design space of the TAURUS dispersed models.

The test mode shapes and frequencies are calculated from a set of hammer tests performed at JSC. The modes up to 150Hz are determined via standard methods.

3000 dispersed models are created and their mode frequencies and shapes are calculated up to 150Hz. Only the first 20 modes are used when comparing the model dispersions to the test data. The dispersions are plotted against the test data as in Fig. 10. The criteria used to compare the TAURUS dispersions are frequency error and mode shape error, as discussed above. After plotting the dispersions, the Pareto front is highlighted in green as in Fig. 10. The dispersions that lie on the Pareto front and their mode shape and frequency errors are given in Table 10. The dispersions that lie on the Pareto front can all be said to be the "best" dispersion, so the RSS norm of the matrix is used as a tie-breaker to pick one dispersion for further model tuning. From Table 10 Pareto-optimal dispersion with the lowest RSS norm value is dispersion 372.

Table 10: Pareto front ids with mode shape and frequency metrics

Dispersion #	Euclidean Norm Value	Frequency Error	RSS Value
2275	1.01	6.96	2.00
2640	1.007	9.10	2.01
372	1.007	11.97	1.93
1251	0.986	12.08	1.99
1792	0.952	16.52	2.04

Dispersion 372 is highlighted in Fig. 10. An alternative method to picking one of the Pareto points would be to change the weighting factors in the frequency and modes shape error metrics.

After selecting TAURUS dispersion 372 for the possible dispersions, it is used as the starting point for further optimization in Attune. As with the dispersions, each of the springs' degrees of freedom are treated as the design variables. However, only variables with a design sensitivity greater than the default threshold are kept in the optimization process. Each design variable is allowed to vary ±20% from the dispersion 372 values. The optimization runs through 100 generations with a population size of 1984. The optimized dispersion is plotted in Fig. 10 along with the hand-tuned version of the TAURUS. The Attune optimization process does not seem to make the model better and in fact makes it worse in the mode shape error metric. However, the Attune code uses the RSS norm of the mode shape error as part of the objective function

rather than the Euclidean norm. Plotting of the model dispersions as a function of the RSS norm, as in Fig.

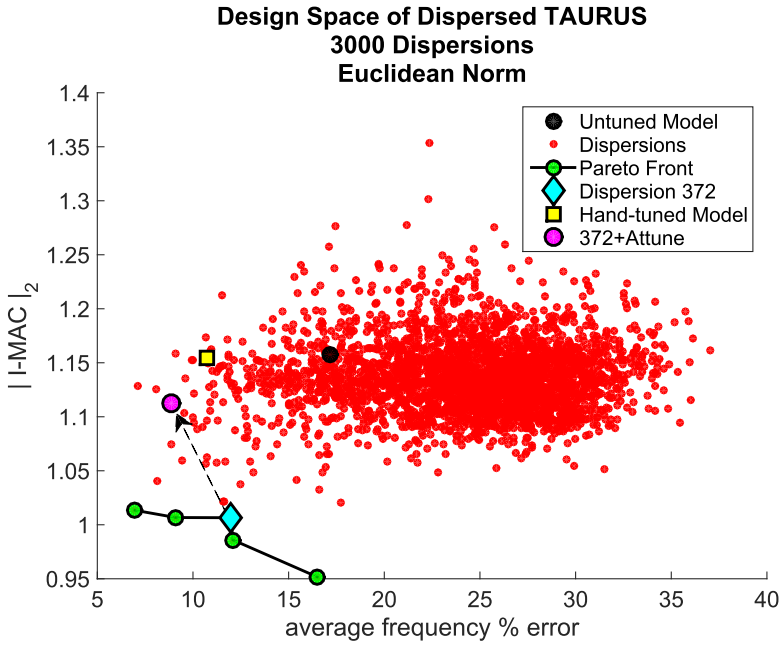

Figure 10: TAURUS dispersion plotted against test data with Pareto front model, hand-tuned model, and Attune model highlighted

11 shows that the Attune does improve the model in the frequency error metric while keeping the overall mode shape error nearly the same.

As with the cart model, the dispersion based model tuning process saves time over the hand-tuning process. The hand-tuning process of the TAURUS relied on building a three-dimensional FEM using it to tune the interface springs. The model dispersion method cuts the model tuning time and produces a correlated model that predicts the test modes better than the hand-tuned model.

C. Ares I-X

For the Ares I-X flight model dispersions, only material and spring properties used for model correlation by Horta, et al.[5] are varied during the dispersion process. The material properties include the Young's modulus for the LAS, Upper Stage Simulator, First Stage, Aft Skirt Stiffener, Forward Skirt Ext and Frustrum, XL and Forward Skirt, and Aft Skirt Shell. Application regions for these material properties can be seen in Fig. 12. The spring properties include the K1, K2, and K3 stiffnesses for the Upper Stage Simulator Springs regions 1 and 2, as shown in Fig. 13. Material properties are randomly varied with a uniform distribution between $\pm 20\%$ while spring properties vary between$\pm 100\%$.

For modal testing, the Ares I-X flight vehicle was placed on top of the mobile launcher, supported by the four hold-down posts, and excited using 4 hydraulic actuators. From the resulting test data, frequency, damping, and mode shapes for all target modes below 12.5 Hz are estimated as described by Horta, et al.[5]

2177 dispersions for the Ares I-X flight vehicle are plotted using the same error criteria and Euclidean norm discussed above and shown in Fig. 14. Dispersed model shapes and frequencies are calculated up to 50 Hz. However, only the first 7 test modes were compared with the first 20 model modes in Fig. 14. Similar to the cart dispersions, the tuned model is shown in yellow, the nominal model is shown in black, and the Pareto Points are shown in green. The Pareto points show a significant improvement from the nominal model in both frequency and mode shape error.

The nominal model and two Pareto points, dispersions 1339 and 1995, are chosen as starting points for one iteration of Attune optimization. During the Attune optimization process for the nominal and chosen Pareto models, the same 7 Young's moduli and 6 spring constants used in the dispersion process are treated

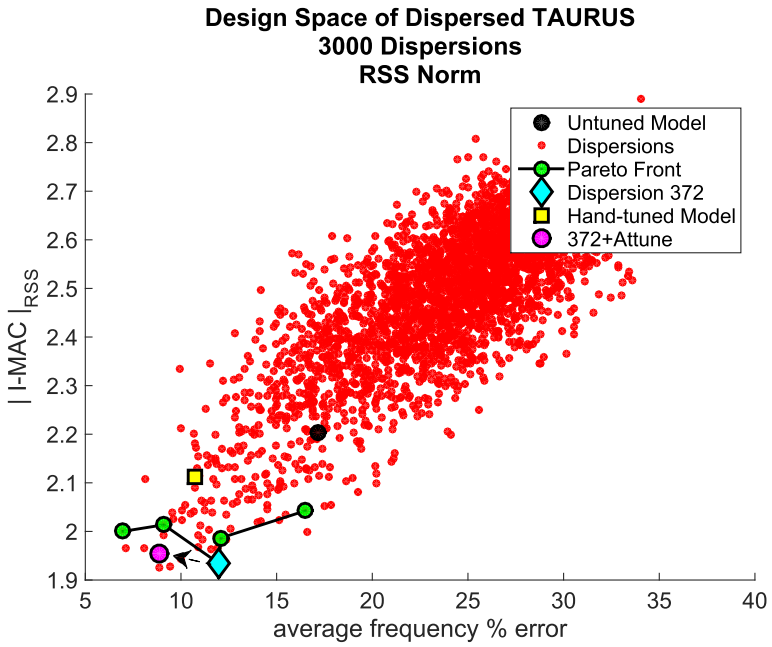

Figure 11: TAURUS dispersions using the RSS norm of the mode shape error

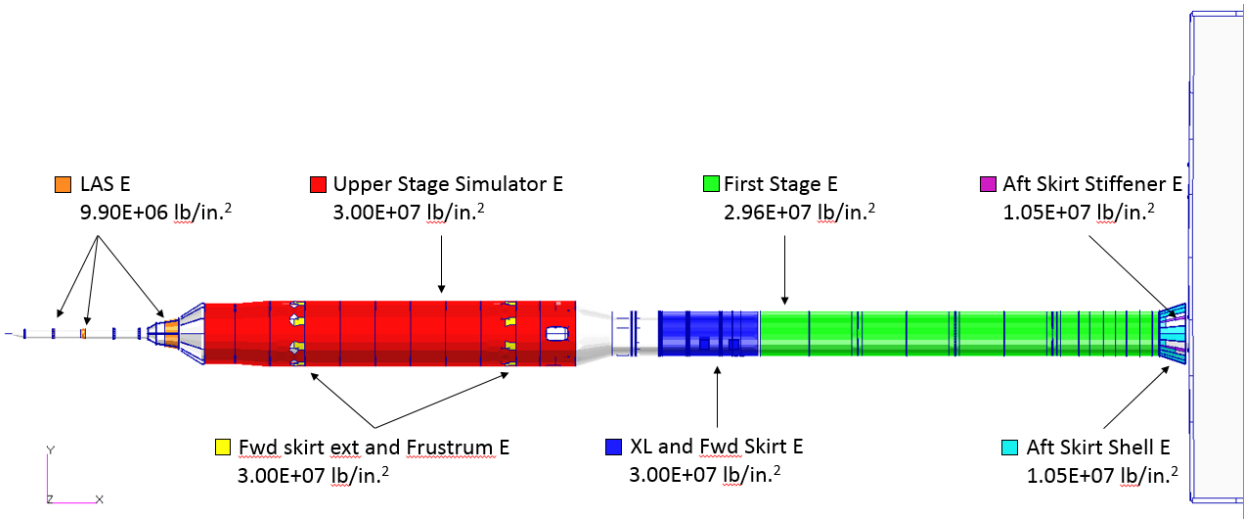

Figure 12: Ares I-X nominal material properties

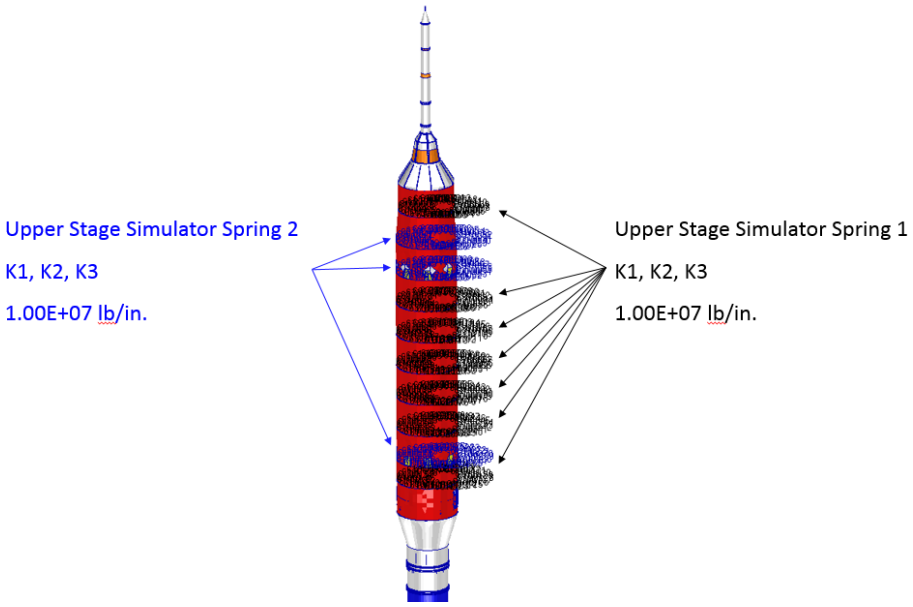

Figure 13: Ares I-X nominal spring properties

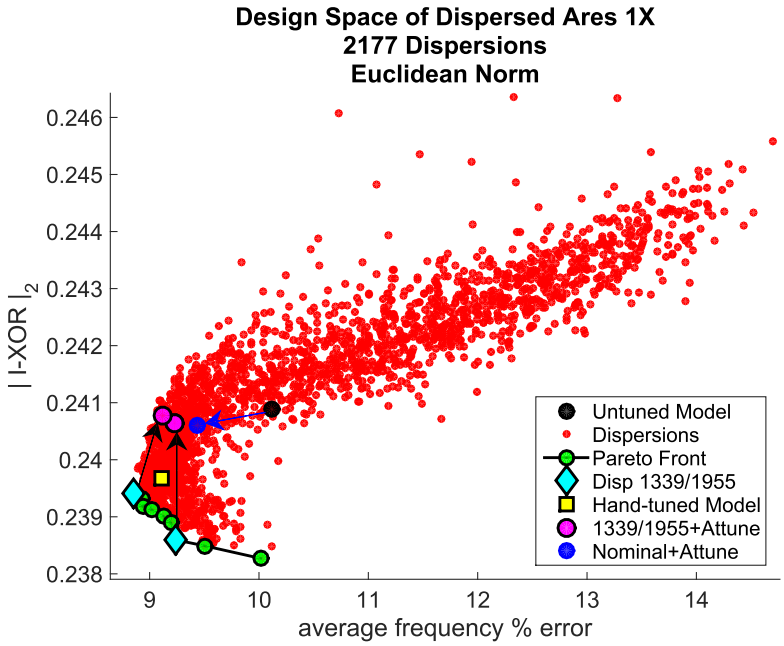

Figure 14: Ares I-X dispersions with the Pareto front highlighted

as design variables. The Young's moduli are allowed to vary ±20% from the dispersion while spring design variables are allowed to vary from 0% to 2000% of the dispersed value. The Attune optimized nominal model is shown in blue while the Attune optimized Pareto models are shown in magenta. The Attune optimized nominal model frequency and mode shape error appear to improve using the Euclidean norm as shown in Fig. 14. However, the Attune optimized Pareto models do not appear to get better. Attune only includes the error in the diagonals of the MAC/XOR matrix when optimizing, while the MAC/XOR error calculation in the Euclidean norm plots includes both the on and off diagonal errors. Fig. 15 shows the 2177 Ares I-X

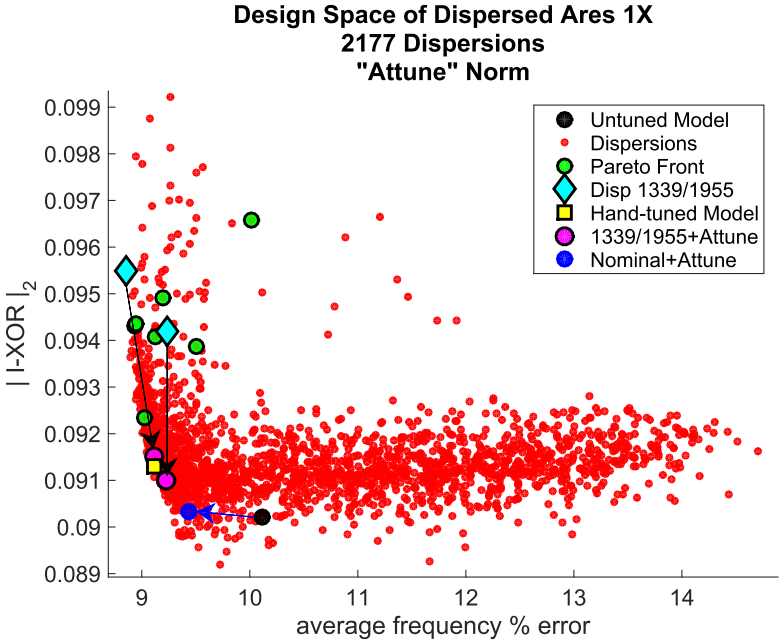

Figure 15: Ares I-X dispersions with the fine-tuned models plotted against the error metrics

flight model dispersions plotted with the MAC error criteria that Attune uses. Using this criteria, all three Attune optimized models come very close to the hand-tuned model and show significant improvement in frequency and shape error over the nominal model.

V. Discussion and Conclusions

This paper introduces a novel method of model correlation. The method begins by creating thousands of pre-test, dispersed models which are then compared against modal test data. Using mode frequency and mode shape error the Pareto front of best models is identified. Using a tie-breaker, one dispersed model is then used as a starting point for model refinement using a model optimization software.

Three structures were used as examples to show the benefits of the current process: a metal cart, the TAURUS, and Ares I-X. This paper shows how the three nominal models are improved by using the dispersed model based correlation methodology. In the cases of the TAURUS model and the cart model, the final correlated model outperforms the hand-tuned model. In the case of Ares I-X, the final tuned models predict the test mode frequencies better than the hand-tuned model but do not predict the mode shapes as well as the hand-tuned model.

This dispersed modes method saves the analyst time during the post-test model correlation phase, and in a scenario where there is not much time allowed for model correlation this method can be used.

References

[1]Tuttle, R. E., Hwung, J. S., and Lollock, J. A., "Identifying Goals for Ares 1-X Modal Testing," *Proceedings of the IMAC-XXVIII*, Jacksonville, FL, February 1-4 2010.

[2]"NASA-HDBK-7005, "Dynamic Environmental Criteria"," March 2001.

[3]Buehrle, R. D., Templeton, J. D., Reaves, M. C., Horta, L. G., Gaspar, J. L., Bartolotta, P. A., Parks, R. A., and Lazor, D. R., "Ares I-X Launch Vehicle Modal Test Overview," *Proceedings of the IMAC-XXVIII*, Jacksonville, FL, February 1-4 2010.

[4]Allemang, R. J., "The Modal Assurance Criterion - Twenty Years of Use and Abuse," *Sound and Vibration*, August 2003, pp. 14–21.

[5]Horta, L., Reaves, M., Buehrle, R., Templeton, J., Lazor, D., Gaspar, J., Parks, R., and Bartolotta, P., "Finite Element-Model Calibaration for Ares I-X Flight Vehicle," 2011.

[6]Parker, G. R. and Ujihara, B. H., "Calculating Cross-Orthogonality with Expanded Test Data," *AIAA Journal*, Vol. 20, No. 9, 1982, pp. 1310.

[7]Guyan, R. J., "Reduction of Stiffness and Mass Matrices," *AIAA Journal*, Vol. 3, No. 2, pp. 380.

[8]Haftka, R. T. and Gürdal, Z., *Elements of Structural Optimization*, Kluwer Academic Publishers, 3rd ed., 1992.

[9]Engineering, A., *Attune*, ATA Engineering, Inc., 2016.

[10]Avitabile, P., "Twenty Years of Structural Dynamic Modification - A Review," *Sound and Vibration*, January 2003, pp. 14–25.

Acknowledgements

Special thanks to Rodney Rocha and Michael Grygier at Johnson Space Center for providing the TAURUS model and to Mercedes Reaves for providing the Ares I-X model.